Microelectronics Reliability 88–90 (2018) 846–854

Contents lists available at ScienceDirect

Microelectronics Reliability

journal homepage: www.elsevier.com/locate/microrel

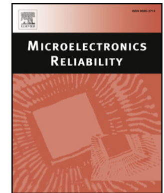

Reliability assessment and failure mode analysis of MEMS accelerometers for space applications

I. Marozau[a,*], M. Auchlin[a], V. Pejchal[a], F. Souchon[b], D. Vogel[c], M. Lahti[d], N. Saillen[e], O. Sereda[a]

[a] CSEM SA, Rue Jaquet-Droz 1, Neuchâtel CH-2002, Switzerland
[b] CEA-LETI, MINATEC Campus, Rue des Martyrs 17, Grenoble Cédex F-38054, France
[c] Fraunhofer ENAS, Technologie-Campus 3, Chemnitz D-09126, Germany
[d] VTT, Kaitovayla 1, P.O. Box 1100, Oulu FI-90571, Finland
[e] ESA ESTEC, Keplerlaan 1, PO Box 299, Noordwijk NL-2200 AG, The Netherlands

ARTICLE INFO

Keywords:
MEMS
Reliability
FMEA
Space application

ABSTRACT

In the present work, the reliability assessment of capacitive MEMS accelerometers of 3 different suppliers (codenamed A, B, and C) for their use in space applications was performed. The developed reliability assessment testing program addressed specific severities of space missions, such as mechanical shocks and vibrations during take-off and rocket stages separation, high temperature gradients and radiation endurance during in-orbit operation. The main aim of the testing was to evaluate the robustness and reliability limits of MEMS devices by overstressing their specific properties through dedicated tests. Typical failures modes were analyzed and root-causes identified on the devices' subsystem level: MEMS structure, ASIC, interconnecting wires, and package. Overall results of the performed reliability assessment tests and failure mode analyses suggest that the most specific MEMS components, namely the microstructures, do not themselves constitute the failure causes. Following the observations, other components, e.g. interconnects, ASIC or packaging, exhibit lower reliability limits to the specific stresses of the space harsh conditions. Comparative analysis of three accelerometers from various suppliers (designs A, B, and C) suggests the design A (in a hermetic ceramic package) to exhibit the best overall reliability for space-specific application conditions. Design B also shows good robustness. However, its non-hermetic packaging makes it unsuitable for the direct use for space applications in the current state. Utilization of a hermetic package and improvement of the wire-bonding temperature resistance would significantly improve this design. Accelerometers of supplier C (in a hermetic ceramic package) have a trend of occasional "infant mortality" early failures. It is therefore very important to perform burn-in and initial prescreening for these devices. Another strong weak point for this design is related to a low radiation endurance, which shall be significantly improved.

1. Introduction

Microelectromechanical systems (MEMS) offer new functionalities and performance advantages over the conventional mechanical and electronic systems due to their dramatically lower mass, lower power consumption, smaller volume, and the possibility of tight integration with electronics [1]. Operation of MEMS devices is based on a wide variety of physical principles for sensing and actuation. The most common being electrostatic, thermal, magnetic, and piezo-electric. MEMS have proven themselves in Earth-based applications such as automotive, biomedical, and electronics by showing outstanding performance and reliability figures [2]. MEMS also have a large potential in space applications like communication, navigation, Earth observation and scientific mission by:

- Fostering new types of scientific missions and instruments (mission-enabling property)
- Reducing cost, size, mass and time from mission conception to launch
- Increasing performances, reliability and redundancy.

* Corresponding author.
E-mail addresses: ivan.marozau@csem.ch (I. Marozau), maxime.auchlin@csem.ch (M. Auchlin), vaclav.pejchal@csem.ch (V. Pejchal), f.souchon@cea.fr (F. Souchon), dietmar.vogel@enas.fraunhofer.de (D. Vogel), markku.lahti@vtt.fi (M. Lahti), nicolas.saillen@esa.int (N. Saillen), olha.sereda@csem.ch (O. Sereda).
URL: http://www.csem.ch (I. Marozau).

https://doi.org/10.1016/j.microrel.2018.07.118
Received 13 July 2018; Accepted 15 July 2018
0026-2714/ © 2018 Published by Elsevier Ltd.

However, until today only a few categories of MEMS components have been or are planned to be used in space applications [1]. Despite the growing interest for this new technology for space and the great reliability figures showed by sensors for Earth-based application, specific space MEMS components still have a relatively low technology readiness level (TRL) [3]. One important reason for this low TRL is the lack of possibility to assess the reliability of MEMS components in a standardized fashion besides than relying on historical standards (such as MIL or ESCC), designed for microcircuits or semi-conductor devices. The lack of appropriate standards specifically written for MEMS components, on which industrials could base themselves for future development and space usage, is therefore of utter interest. Reliability assessment of MEMS for space applications shall, on one hand, take into consideration particularities of the design and structure of MEMS devices in comparison to their conventional mechanical and electronic counterparts. MEMS typically combine micro-scale mechanical components with electronics. Typical MEMS device consists of:

– One or several micron-sized sensors, which detect the specific natural events or changes in the environment and generate raw signal (s)
– Application-specific integrated circuit (ASIC) that processes the raw sensor signal
– Interconnecting wires
– Device package and underlying joining techniques.

The test program shall therefore target the reliability of these constituents. On the other hand, this evaluation shall also take into account specific requirements for space applications, such as intense mechanical shock and vibrations during launch, high temperature gradients, and radiation effects during in-orbit operation [4].

The present work was dedicated to reliability assessment and comparative analysis of MEMS capacitive accelerometers. The reliability evaluation was performed according to the developed standardized testing methodology for reliability assessment of MEMS as required for space applications [5]. The main aim of the testing was to evaluate the robustness and reliability limits of MEMS devices by overstressing their specific properties and parameters with dedicated tests, such as thermal cycling, mechanical shock, mechanical vibrations, humidity resistance, or radiation endurance.

Accelerometers from three different suppliers (codenamed A, B, and C) were tested, and their reliability figures were compared. Among the chosen accelerometer types, devices from the suppliers A and C were hermetically sealed using a ceramic package and devices from the supplier B were sealed non-hermetically in a plastic package filled with gel. Accelerometers from the suppliers A and B were three-axis, whereas devices from the supplier C were two-axis. In order to understand the critical accelerometer design weaknesses, failure root cause analysis has been performed for the selected failed devices. The results have been compared between the different accelerometer types and general suggestions were drawn on the improvement of the device robustness for space applications.

2. Reliability assessment concept

Identical test program was followed for the accelerometers from the suppliers A, B, and C. The program was based on the existing military and space standards (MIL and ESCC) for electrical components and integrated circuits [5], as well as on the specially-developed space standard for MEMS [6]. A set of 150 devices was selected from a homogeneous production lot for each of the evaluated MEMS manufacturer. The selected devices were not subject to any pre-screening. The reliability assessment test program consisted of 3 successive phases (Fig. 1):

1. **Initial Inspection**. Performed for all samples in order to identify their conformity to the basic specifications and replace the failed devices prior to the Testing Phase.
2. **Testing Phase**. Consisted of various reliability assessment tests. The main objective was to overstress specific characteristics of the MEMS devices, with aim to determine the reliability limits and detect the possible failure modes. All samples were randomly divided into sub-groups per each test as shown in Fig. 1.
3. **Final Inspection**. Performed in order to identify failed MEMS devices that were not identified during the Testing Phase.

Failure identification was carried out during the intermediate failure assessment test interruptions and at the end of each test. The failure criteria was the deviation of any accelerometer parameters of more than 5% from their original values obtained during the Initial Inspection phase. The corresponding accelerometer parameters taken into account were device signals at the applied acceleration levels of $+1\,g$, $-1\,g$ and $0\,g$ in each of the accelerometer primary axes (X, Y, Z for the designs A and B; X, Y for the design C).

Devices failing during the testing phase were submitted to a failure modes and effects analysis (FMEA) procedure. Failed accelerometers were analyzed with respect to mechanical/electrical failures of the MEMS dies, interconnects, and package. Specific ASIC faults were not investigated within the scope of this work.

3. Experimental details

Unless otherwise specified, all tests and measurements were carried out under the following normal atmospheric conditions:

– Room temperature: (22 ± 3) °C
– Relative humidity: (55 +10/ −20) %
– Atmospheric pressure (1 bar)

Two-step stress tests

A two-step procedure was applied to the following environmental and mechanical tests (Fig. 1):

– Temperature cycling
– Mechanical shock
– Mechanical vibration
– Pressure cycling

The procedure is comprising of two steps:

- *Step 1*. Analysis of the failure sensitivity to load in order to identify the device reliability limit(s) and define the load parameter to be applied in Step 2.
- *Step 2*. Acquisition of failure statistics over cycles by applying the load parameter defined based on the results of Step 1. This step involves repetitive load cycling tests at a fixed load until failure as per the criteria defined above.

This two-step procedure was applied in order to measure not only the accelerometer reliability limits, but also to evaluate the failure statistics over load cycles when the devices operate close to their reliability limits. This would allow to predict the failure rates and devices lifetime when they are exposed to such severe load conditions.

In Step 1, for each of these tests the device ***failure load limit*** was first determined on a series of 5 samples. These specimens were tested with increased load parameter. The load parameter value at which more than 50% of the tested devices failed corresponds to the ***failure load limit*** for the particular test. The load parameter to be applied in Step 2 was obtained by reducing the ***failure load limit*** by a certain factor (specific for each particular test). Acquisition of failure statistics over cycles in Step 2 was performed by testing of a series of 15 samples at this load level. The devices were tested by exposing them to an

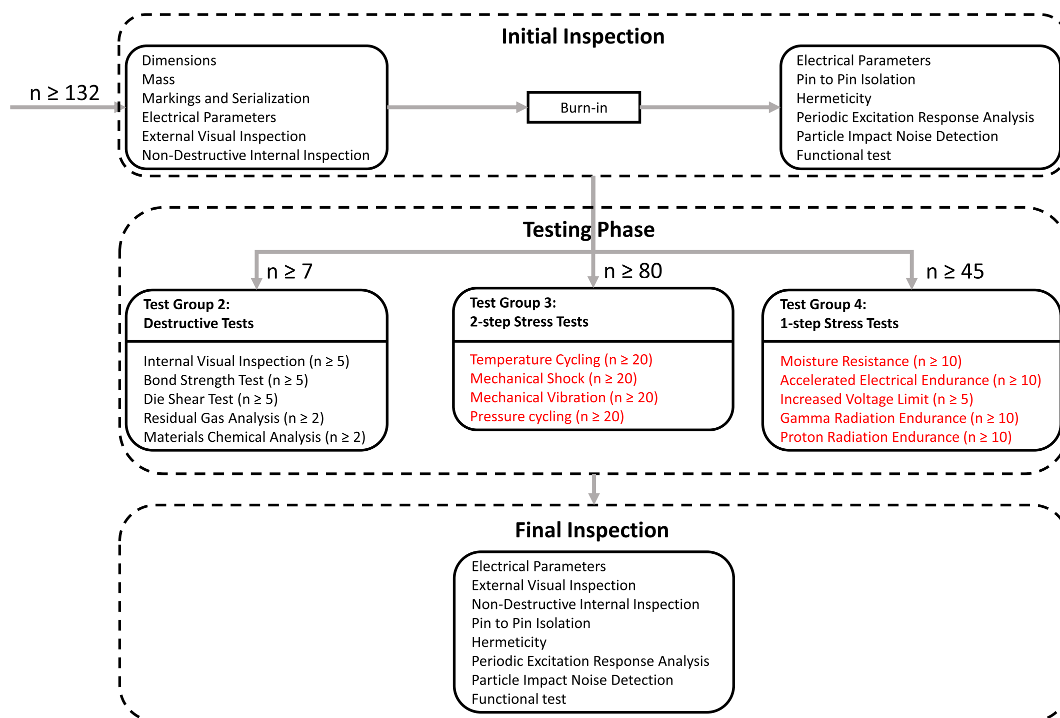

Fig. 1. Test program scheme. The highlighted lines correspond to the tests performed in the present study.

increased number of test cycles in specified iteration steps. After each step, intermediate functional measurements of all tested samples were carried out for the failures check. All failed devices (as per the aforementioned criteria) were registered and removed from the next iteration step. The test continued until all samples failed or until the maximum specified number of cycles was reached. Statistical analysis of the Step 2 test results was performed using a Weibull failure distribution model combined with a Kaplan-Meier parametric estimation approach [7].

3.1. Temperature cycling test

The test was performed using a CTS TSS-70/130/S double chamber system according to the standards [MIL-STD-883J Method 1010]. The sample basket was moved between the high- and low-temperature chambers, which were kept at constant specified temperatures T_{hot} and T_{cold}, respectively. The transfer time was about 10 s. The total dwell time at each temperature (T_{hot} and T_{cold}) was 20 min. This time was sufficient to allow thermal equilibrium inside the device package.

3.2. Mechanical shock test

The test was performed using a Yoshida Seiki PST-300 pendulum shock testing machine. The samples were rigidly mounted on the back side of the pendulum, which then hits the stopper bumper. The shock acceleration was controlled by an external calibrated accelerometer mounted close to the tested devices. The shock acceleration profile had a nearly half-sine shape with a pulse duration of about 0.2 ms. The used equipment allowed to reach shock accelerations up to 5000 g.

3.3. Mechanical vibration test

The test was performed using a mechanical shock/vibration test equipment SW 3710 with PDM rectifier TGE 10-1 according to the standard [MIL-STD-883J Method 2007]. The samples were rigidly mounted on a sample holder. The peak acceleration was measured by an external calibrated accelerometer mounted next to the tested devices. The acceleration profile had a quasi-sine shape. The total time of one sweep cycle from 20 Hz to 2000 Hz was 4 min. The used equipment allowed to reach a maximum peak acceleration of 41.6 g.

3.4. Pressure cycling test

The test was carried out according to the standard [ECSSEST3202] using a setup designed and manufactured at CEA-LETI. The system is capable of controlling the specified pressure profile in the test chamber. The test was performed by cycling the pressure from P_{low} = 1 bar up to the specified high pressure set point P_{high} (max 7.75 bar) and back using nitrogen or helium as working gases. The dwell time at 1 bar and at the high pressure was 60 to 70 s, the pressure ramp up and ramp down time was 10 to 20 s.

3.5. Moisture resistance test

The test was performed according to the standard [MIL-STD-883J method 1004] using a CTS thermal testing equipment CSR-60/600-5 equipped with a separated climate test box. The test procedure was as follows:

1. Relative humidity (RH) inside the chamber was set to 95% and temperature was increased to 65 °C.
2. After reaching 65 °C the temperature was kept at this value for 3 h (RH = 95%).
3. Temperature was decreased to 25 °C.
4. Temperature was increased to 65 °C.
5. Temperature kept at 65 °C for 3 h (RH = 95%).
6. Temperature was decreased to 25 °C.
7. Temperature kept at 25 °C for 3 h(RH = 95%).

Steps 1 to 7 constitute one cycle of the moisture resistance test. For every second test cycle, in the steps 6 and 7 the temperature was decreased to −10 °C (instead of 25 °C) and kept for 3 h. During this low temperature steps the humidity was not controlled.

3.6. Accelerated electrical endurance test

The test was carried out according to the standard [ESCC 226900] using a setup designed and manufactured at CSEM. The test was performed by operating the devices at temperatures exceeding their maximum specified temperature of operation. The samples were divided in three groups for the tests at three different temperatures $T_1 < T_2 < T_3$. The total test duration for the temperatures T_1, T_2, and T_3 was 1000 h, 500 h and 168 h, respectively.

3.7. Increased voltage limit test

A series of 5 devices was tested for each supplier. The test was performed under normal atmospheric conditions by subjecting the accelerometer devices to increased drive voltage starting from the standard voltage from the suppliers' datasheets, with incremental steps between 10% and 50% (see more details in the Results and discussion 4 section). For each step, the voltage was applied for one hour followed by the device failure assessment. The test continued until all devices failed.

3.8. Radiation endurance tests

Gamma and proton radiation endurance tests were performed. Gamma radiation endurance test was carried out according to the standard [ESCC 22900] at the Co-60 gamma radiation facility at ESTEC[1]. The average gamma radiation dose rate (for Si) during the irradiation runs was about 2.35 ± 0.12 krad/h. For each MEMS supplier, the sample set consisted of 10 accelerometers. The sample sets were divided in 4 groups irradiated with different radiation doses: 2 samples at 10 krad, 2 samples at 20 krad, 3 samples at 55 krad, and 3 samples at 110 krad.

Proton radiation endurance test was carried out according to the standard [ESCC 22900] at the proton irradiation facility at PSI[2] using a 50 MeV proton beam. The average proton radiation dose rate and flux (for Si) during the irradiation runs were about 35 rad/s and $2.2 \cdot 10^8\,\mathrm{p\,cm^{-2}\,s^{-1}}$. The sample sets were divided in 4 groups irradiated with different radiation doses: 2 samples at 10 krad, 2 samples at 20 krad, 3 samples at 50 krad, and 3 samples at 100 krad.

3.9. Failure mode analysis

Analysis of failure modes was performed on the failed samples for the selected reliability tests: temperature cycling, mechanical shock, pressure cycling, and radiation endurance. For each supplier, a few samples with the most typical failure signature were subjected to the analysis. Two major approaches were applied for the failure mode analysis:

– Non-destructive inspection by X-ray imaging/tomography aiming at the detection of the relevant failure sites (wire bonding, die and package assemblies, hermeticity loss, etc.);
– Destructive analysis consisting of opening the device package and subsequent inspection by optical microscopy (OM) and/or by scanning electron microscopy (SEM).

The identified failures were related to the design features and possible weaknesses.

[1] European Space Research and Technology Centre (ESTEC), European Space Agency, Noordwijk, The Netherlands.

[2] Paul Scherrer Institute, Villigen, Switzerland.

4. Results and discussion

4.1. Temperature cycling

The purpose of this test was to evaluate the ability of the devices to withstand mechanical and other stresses induced by alternating temperature between high and low extreme values. In particular, temperature cycling causes thermal expansion and contraction of constituting materials, which can induce cyclical mechanical stresses. The subsequent fatigue and may lead to permanent changes in electrical and/or physical characteristics of the tested devices.

Step 1 of the temperature cycling test (determination of the failure load limit) was performed on a batch of 5 samples for each supplier. The devices were subjected to 5 temperature cycles with successively increased temperature difference $\Delta T = T_{hot} - T_{cold}$. The test continued until at least 3 out of 5 tested devices failed or until the maximum equipment ΔT of 315 °C (+250 °C / −65 °C) was reached. Accelerometers of the supplier A exhibit a very good stability for temperature cycling. None of the 5 tested devices failed up to the maximum equipment ΔT of 315 °C. On the other hand, design B appeared more prone to failure: after successfully passing the test at a ΔT of 260 °C(+200 °C / −60 °C), 3 over 5 of those accelerometers failed during the following step, at ΔT of 280 °C(+220 °C / −60 °C), thus making ΔT = 280 °C the failure load limit for the design B. Accelerometers of the supplier C showed an intermediate stability for temperature cycling. One C device failed immediately after the first test step at a ΔT of 185 °C, which points to a probable early case failure due to missing burn-in of the devices [8]. Because the required number of minimum 3 failed accelerometers was not reached, the temperature gap was successively increased up to the maximum equipment ΔT of 315 °C. No additional failures was observed for any of these load steps.

Acquisition of failure statistics over cycles (step 2 of the temperature cycling test) was performed at similar ΔT of 250–260 °C for all three suppliers for the sake of consistency. This ΔT corresponds to about 90% of the failure load limit for the supplier B devices that showed a lower stability to temperature cycling in comparison to suppliers A and C. The chosen ΔT was realized by keeping T_{cold} = −65 °C and lowering T_{hot} down to 185–195 °C in order to avoid potential detachment of interconnecting wires form the bonding pads, which was found to be the main failure mode for the supplier B devices.

A batch of 15–20 samples per supplier was subjected to the increasing number of cycles with a step of 10–50 cycles. The test continued until all devices failed or a total number of 500 cycles (400 for the supplier B) was reached. Fig. 2 shows the number of survived devices as a function of the number of temperature cycles per supplier. Designs A and C exhibit a slow failure rate with the number of cycles with more than 50% of the batch survived after 500 temperature cycles. On contrary, design B shows a much higher failure rate with a large number of devices failing around 100 cycles. This is in line with the previous findings of the step 1 of the test, where supplier B devices also show the worst performance. The acquired data was statistically analyzed using a Weibull failure distribution model combined with a Kaplan-Meier parametric estimation approach [7].

Fig. 3 shows the results of the statistical analysis of the temperature cycling test data per accelerometer supplier. Designs A and C reveal a high characteristic life parameter of 1270 ± 200 and 1670 ± 300 cycles and, respectively, which is much higher than the characteristic life of supplier B device of 390 ± 60 cycles, which again supports the previous findings. The Weibull shape parameter for the designs A and C is less than 1, suggesting a general decrease of the failure rate with the number of temperature cycles. This is also supported by the large number of non-failed devices after the test's end (see Fig. 2). The Weibull shape parameter for the accelerometer design B is very close to 1, indicating a nearly constant failure rate over the number of temperature cycles. However, the presence of a large number of failure events happening around 100 cycles (Fig. 2) and a significant deviation

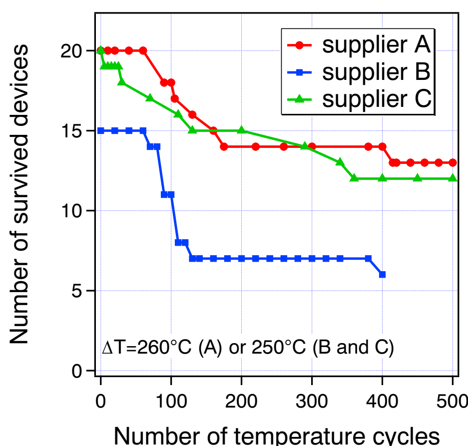

Fig. 2. Number of survived devices in temperature cycling test as a function of the number of temperature cycles at the specified temperature conditions for the suppliers A, B, and C. Each data point represents a failure assessment step.

of the model fit from the experimental data points in this region (Fig. 3) suggests a possible presence of two failure modes. To reveal this scenario, more test samples are required and the tests shall be prolonged to larger number of cycles.

Failure analysis was performed by non-destructive X-ray tomography of the closed packages, and by optical microscopy and SEM observations of the opened packages. All three designs suggest a similar typical failure root case, which is linked to the issues with interconnect wires. The most typical observed damage types are interconnect wire cuts and cracks, wire debonding from the bonding pads or significant weakening of this connection (as confirmed by additional wire-bond pull-tests), and surface contamination by the created debris. These causes can originate from the used bonding technique, wire material and thickness, and excessive mechanical load on the wires. At the same time, failure analysis does not reveal any damage to the MEMS structures or ASICs due to mechanical stresses caused by temperature cycling.

4.2. Mechanical shock

The purpose of this test was to evaluate the MEMS accelerometers ability to withstand severe mechanical shocks, which may be caused by suddenly applied forces or abrupt changes in motion produced by rough handling, transportation, or field operation (e.g. during the take-off or stages separation phases of a rocket flight). The test aims for the determination of the mechanical shock limits of the MEMS structure, package, internal metallizationand lead system, ASIC die, and other elements of the MEMS device.

Step 1 of the mechanical shock test (determination of the failure load limit) was performed on a batch of 5 samples for each supplier. The devices were subjected to 5 shock pulses in each of the six primary directions (X+, X−, Y+, Y−, Z+, and Z−) with successively increased peak acceleration a starting from 2000 g up to 5000 g (equipment limit) with steps of 500 g. Devices from the suppliers A and B exhibit no failures for the entire tested range of the shock acceleration. The result indicates that the failure load limit for a small number of shock pulses exceeds 5000 g. Supplier C devices show a worse mechanical shock resistance, revealing failures over quite a broad range of the shock acceleration. All 5 devices survived shock accelerations up to 2500 g. The first device failed at 3000 g whereas the last one withstood the shock acceleration of 5000 g. The failure load limit for the design C accelerometers equals to 2750 ± 250 g (calculated from the first failure occurrence).

Acquisition of failure statistics over cycles (step 2) was performed at $a = 5000\,g$ for the suppliers A and B, and at $a = 2000\,g$ for the supplier C, which is close to a 75% load of the failure load limit of 2750 g. A batch of 15 samples per supplier was subjected to the increasing number of mechanical shock pulses with increment steps of 90, 300, and 120 pulses for the design A, B, and C, respectively. Fig. 4 shows the number of survived devices as a function of the number of shock pulses per supplier. Supplier A and B devices show a similar behavior with a pronounced acceleration of the failure rate around 500 and 1200 shock pulses, respectively. On contrary, design C (tested at a = 2000 g) exhibits a nearly linear monotonous increase of the failure number as a function of the number of pulses. This indicated that the failure rate has a more moderate time-dependency. The acquired data was statistically analyzed using a Weibull failure distribution model combined with a Kaplan-Meier parametric estimation approach [7]. Fig. 5 shows the results of the statistical analysis of the mechanical shock test data per accelerometer supplier. Designs A and B (which both show a high mechanical shock resistance for small number of pulses) exhibit a significant difference in the characteristic number of pulses (N_C) to failure at a = 5000 g. The long-term stability of the supplier B accelerometers (N_C = 1360 ± 150 pulses) is about twice better in comparison to the supplier A (N_C = 620 ± 50 pulses). Both design reveal a high Weibull shape parameter of 3.2 and 2.9 (Fig. 5). This indicates a typical "wear-out" behavior meaning that the failure rate increases fast after a certain number of shock pulses. Design B accelerometers reveal a much more

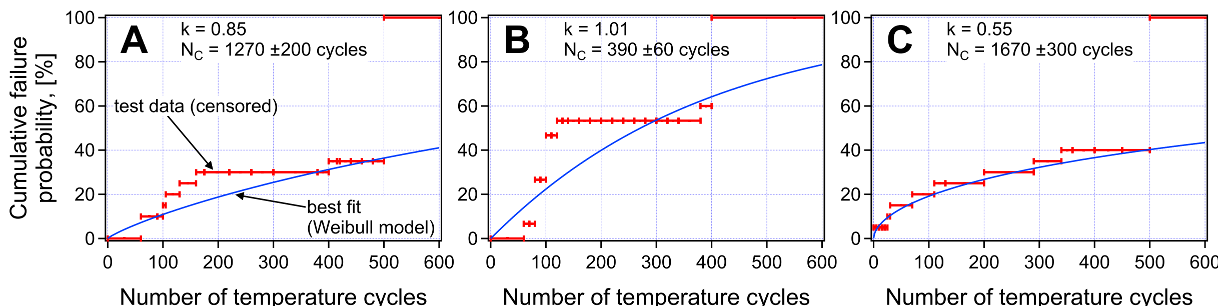

Fig. 3. Results of the statistical analysis of the temperature cycling test data per accelerometer design. Horizontal red strokes represent the raw test data (censored), blue curve is the best fit using a Weibull distribution model. The corresponding Weibull model parameters for each supplier are given on the graph: k is shape factor, N_C is characteristic life (in number of temperature cycles). (For interpretation of the references to color in this figure legend, the reader is referred to the web version of this article.)

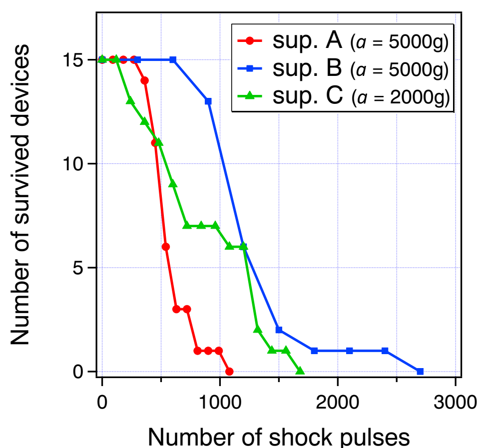

Fig. 4. Number of survived devices in mechanical shock test as a function of the number of shock pulses at the specified peak acceleration for the suppliers A, B, and C. Each data point represents a failure assessment step.

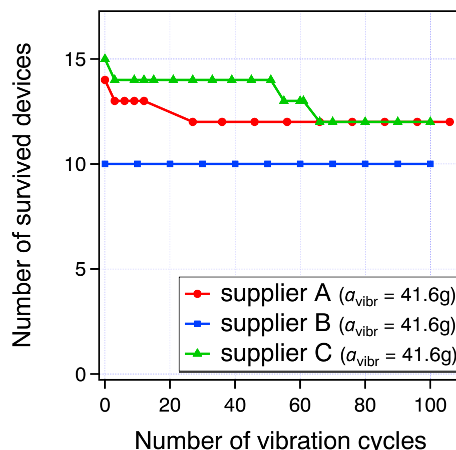

Fig. 6. Number of survived devices in mechanical vibration test as a function of the number of vibration sweep cycles (20–2000 Hz) at the specified peak acceleration for the suppliers A, B, and C. Each data point represents a failure assessment step.

moderate increase of the failure rate with the number of shock pulses (smaller k of 1.9).

The failure root cause for mechanical shock test is identical for all studied devices, namely it is detachment of the interconnect wires from their contact pads inside the packaging. Utilization of the glob top approach (gel-like polymer material to fill the package interior), which is realized in the design B, helps to improve the shock resistance by making the interconnect wires more secured through the reduction of their movement amplitude inside the package. At the same time, failure analysis does not reveal any damage to the MEMS structures or ASICs as a result of high mechanical peak accelerations.

4.3. Mechanical vibration

The purpose of this test was to evaluate the MEMS accelerometers ability to withstand mechanical stresses and fatigue caused by mechanical vibration in the specified frequency range. The test aims for the determination of the mechanical vibration limits of the MEMS structure, package, internal metalization and lead system, ASIC die, and other elements of the MEMS device.

Step 1 of the mechanical vibration test (determination of the failure load limit) was performed on a batch of 5 samples for each supplier. The devices were subjected to 3 frequency-sweep cycles (20 to 2000 Hz) in each of the three primary axes (X, Y, and Z) with successively increased peak acceleration a_{vibr} starting from 18.9 g. The test continued until at least 3 out of 5 tested devices failed or until the maximum equipment a_{vibr} of 41.6 g was reached. Devices from the suppliers A and B exhibit no failures for the entire tested range of the peak acceleration. One supplier C device failed immediately after first test step at a_{vibr} = 18.9 g, which points to a typical early case failure due to infant mortality [8], similar to what was observed in temperature cycling test. Then, because the required number of minimum 3 failed accelerometers was not reached, the peak acceleration was successively increased up to the maximum equipment a_{vibr} of 41.6 g. No additional failures was observed for any of these load steps. The obtained results indicate that the failure load limit for a small number of vibration cycles exceeds 41.6 g for all accelerometer designs. Therefore the failure acquisition over cycles (step 2 of the test) was performed at the maximum equipment peak acceleration of 41.6 g. A batch of 10–15 samples per supplier was subjected to the increasing number of vibration cycles with a step of 3–10 cycles. The test continued until all devices failed or a total number of 100 cycles was reached. Fig. 6 shows the number of survived devices as a function of the number of vibration cycles per supplier. All tested designs exhibit a good mechanical vibration resistance and slow failure rates with the number of cycles. Only a few failures for the designs A and C were observed. Such low failure rates do not allow to acquire enough data to perform an accurate statistical analysis. Similar to the mechanical shock tests results, design B seem to show the best resistance for the mechanical effects caused by vibrations.

4.4. Pressure cycling

Pressure cycling test intends to verify the resistance of device and in particular its package to a repeated increase and decrease of pressure. This test accelerates leakage failures in hermetically sealed devices. Pressure cycling is performed using nitrogen or helium gases. Helium

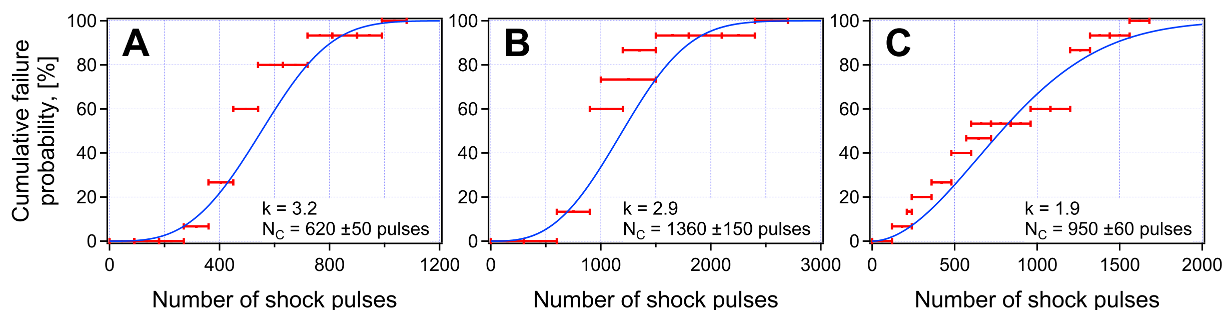

Fig. 5. Results of the statistical analysis of the mechanical shock test data per accelerometer design. Horizontal red strokes represent the raw test data (censored), blue curve is the best fit using a Weibull distribution model. The corresponding Weibull model parameters for each supplier are given on the graph: k is shape factor, N_C is characteristic life (in number of shock pulses). (For interpretation of the references to color in this figure legend, the reader is referred to the web version of this article.)

penetrates easier inside the package due to its smaller molecular size and, therefore, may induce faster leakage failures.

Step 1 of the pressure test (determination of the failure load limit) was performed on a batch of 5 samples for each supplier. The devices were subjected to 20 pressure cycles with successively increased overpressure ΔP starting from 2.0 bar (using nitrogen). The test continued until at least 3 out of 5 tested devices failed or until the maximum equipment ΔP of 6.75 bar was reached. If the samples passed the test with nitrogen gas, then the same test procedure was repeated using helium. For the interpretation of the test results it is important to keep in mind that devices from the suppliers A and C are hermetically sealed in a ceramic package, whereas supplier B devices are sealed non-hermetically using a plastic package. Suppliers A and C devices exhibit very good pressure cycling resistance. No samples of them failed up to the maximum overpressure of 6.75 bar for both nitrogen and helium gases. The pressure cycling resistance of the supplier B devices is significantly lower: an expected result considering its non-hermetic package. 2 out of 5 design B accelerometers failed at a nitrogen overpressure of 4.5 bar with two more accelerometers failing after the next step at $\Delta P(N_2)$ of 6.75 bar. The failure load limit for the design B is therefore $\Delta P(N_2) = 6.75$ bar.

The failure acquisition over cycles (step 2 of the test) was performed for a batch of 15 devices per supplier. Design A and C accelerometers were tested at the maximum equipment overpressure of 6.75 bar using nitrogen. This maximum possible overpressure was applied since the failure load limit is even greater and could not be determined. Design B accelerometers were tested at four progressively increasing applied overpressure corresponding to 50%, 60%, 75% and 90% of the failure load limit of 6.75 bar. All devices that successfully passed the test were subjected to the next step with increased overpressure as described above. The test continued until all devices failed or a total number of 200 pressure cycles was reached. All accelerometers of the suppliers A and C survived after 200 pressure cycles using the maximum overpressure of 6.75 bar. This high resistance indicates a very good quality of the packaging technology in both designs. Fig. 7 shows the number of the survived design B accelerometers in pressure cycling test as a function of the number of cycles at the specified ΔP. The devices exhibit a slow progressive failure occurrence with the number of cycles. The increase of the applied overpressure does not accelerate the failure rate for the survived samples. The observed low failure rates do not allow to perform its accurate statistical analysis. The most typical failure signature is the signal offset drift (0 g signal) while the device sensitivity remains quite stable. Root cause failure analysis of the supplier B devices did not reveal any visible damage to the interconnects. Root cause failure analysis of the supplier B devices did not reveal any visible damage to the interconnects. Most probably the failure mechanism is linked to the loss of MEMS package hermeticity, which causes excessively high pressure and continuous constant mechanical stresses being applied on the sensitive parts of the MEMS structure and/or ASIC components. This could lead to the MEMS structure deformation and cause a drift of the device calibration parameters.

4.5. Moisture resistance

The purpose of the moisture resistance test is to perform an accelerated assessment of the resistance of a device and its constituting parts to the deteriorative effects caused by high humidity and heat. This is required for the device storage and operation in tropical climate environments, such as the main ESA launch site in Kourou, French Guiana. Often the rocket payload is stored for extensive time periods. The moisture resistance test is therefore designed to represent accelerated degradation under such conditions and is of great importance for the reliability assessment of space products. The performed test is different from steady-state humidity tests (e.g. long-time storage at 85 °C /85% RH) by applying alternative periods of condensation and drying (see more details in the experimental section). The severity with respect to corrosion processes is increased. It also includes a low-temperature sub-cycle for revealing the deterioration effects caused by cracks formation. This is achieved by the accelerated crack widening, growth and propagation due to volumetric expansion of the frozen surface moisture.

The total number of test cycles was 10, as specified in the corresponding standard [MIL-STD-883J method 1004]. A test batch consisted of 10 devices per accelerometer supplier. All tested devices of all suppliers successfully passed the test. No failure was observed. The typical deviation of the accelerometer parameters are within 2% for all suppliers. This indicates a very good resistance of the tested accelerometer designs for the deteriorative effects caused by high humidity and heat typical for tropical environments in an accelerated fashion.

4.6. Accelerated electrical endurance

The purpose of this test is to thermally accelerate aging of the MEMS and ASIC components in order to evaluate the stability of the accelerometer operation under the accelerated aging conditions and to analyze the observed failures. The test was carried out for a batch of 10 devices per supplier. The accelerometers were subjected to operation at three different temperatures exceeding their maximum specified operation temperatures (see test temperature conditions in Table 1).

Table 1 shows a comparison of the accelerated electrical endurance tests results between different device suppliers. In general, design B accelerometers exhibit the best performance. Supplier C devices show a reasonably good stability. However, some random catastrophic failures were detected even at lower test temperatures of 85–125 °C, which might be the infant mortality effect due the absence of burn-in, as it was already seen in some other tests of the design C accelerometers. Supplier A devices reveal a trend of continuously increasing deviation of their parameters during the accelerated electrical endurance tests,

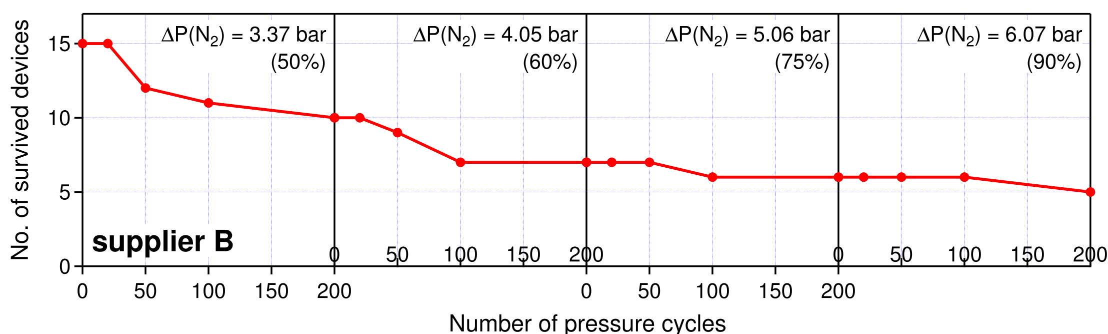

Fig. 7. Number of the survived supplier B devices in pressure cycling test as a function of the number of cycles at the specified ΔP (% of the failure load limit). The test was performed up to 200 cycles at a constant ΔP. All survived samples were successively tested at increased ΔP corresponding to 50%, 60%, 75%, and 90% of the failure load limit. Each data point represents a failure assessment step.

Table 1
Temperature condition and results of the accelerated electrical endurance test: cumulated number of failed samples after the corresponding test step/total number of samples in the test batch. $T_{op,max}$ is the maximum specified operation temperature, T1, T2, and T3 are the temperature test conditions.

Temperature condition	Time	Supplier A	B	C
$T_{op,max}$		**125 °C**	**125 °C**	**85 °C**
T_1		**125 °C**	**125 °C**	**85°C**
	168 h	0/3	0/3	0/3
	500 h	0/3	0/3	1/3
	1000 h	0/3	0/3	1/3
T_2		**165 °C**	**165 °C**	**125 °C**
	168 h	0/3	0/3	1/3
	500 h	1/3	0/3	1/3
T_3		**185 °C**	**185 °C**	**165 °C**
	168 h	1 / 4	0 / 4	0 / 4

which becomes more pronounced at higher temperatures of 165–185 °C. It is noteworthy that both observed design A failures are not catastrophic, but are linked to a signal drift. Therefore, the failure rate would depend on the chosen failure criteria, e.g. on the permitted signal deviation threshold (5% in the present study).

4.7. Increased voltage limit

The test goal was to evaluate the resistance of MEMS devices to the increased drive voltage and to identify the most sensitive for it device component. The tests were performed on a series of 5 samples per supplier by subjecting them to increased voltage conditions in successive steps as shown Table 2. The staring voltage was chosen to be 50% more than the standard operating voltage for the given device design. The observed failure limit voltages are (at least 3 out of 5 failed samples): 7.5 –9.0 V for the supplier A, 8.3 –10.0 V for the supplier B, and 7.5 –9.0 V for the supplier C. All accelerometer designs exhibit similar drive voltage limits. Failure mode analysis suggests that the failures originate from the failing ASIC components. The MEMS structures and interconnects are not damaged during the test.

4.8. Radiation endurance

Two radiation endurance tests were performed in order to evaluate the stability of MEMS accelerometers for the effects of total ionizing dose and/or displacement damage for the steady-state gamma and proton radiation. The possibility of further degradation with time after irradiation was also accommodated in the test procedures. Proton radiation is considered to cause more severe damage to the certain types of integrated circuits in comparison to gamma radiation [9,10].

Table 2
Test conditions and results of the increased voltage limit test. U is the applied drive voltage, N_F/N_T is the cumulated number of failed samples after the corresponding test step/total number of samples in the test batch. The first raw (in bold) represents the standard operation voltage per device supplier.

Supplier A		Supplier B		Supplier C	
U [V]	N_F/N_T	U [V]	N_F/N_T	U [V]	N_F/N_T
2.50		**3.30**		**5.00**	
3.75	0/5	5.00	0/5	7.50	0/5
5.00	0/5	6.70	0/5	9.00	3/5
6.25	0/5	8.30	0/5	10.0	5/5
7.50	0/5	10.0	5/5		
9.00	5/5				

Table 3
Number of failed samples immediately after the gamma/proton irradiation > Number of failed samples after the subsequent room temperature storage > Number of failed samples after the subsequent high-temperature storage/ Number of tested samples at different proton radiation doses for each accelerometer supplier

Supplier	A	B	C
Gamma	Number of failed devices		
10 krad	0 > 0 > 0/2	0 > 0 > 0/2	0 > 0 > 0/2
20 krad	0 > 0 > 0/2	0 > 0 > 0/2	0 > 0 > 0/2
55 krad	0 > 0 > 0/3	0 > 0 > 0/3	1 > 1 > 1/3
110 krad	0 > 0 > 0/3	0 > 0 > 0/3	3 > 3 > 3/3
Proton	Number of failed devices		
10 krad	0 > 0 > 0/2	0 > 0 > 0/2	0 > 0 > 0/2
20 krad	0 > 0 > 0/2	0 > 0 > 0/2	0 > 0 > 0/2
50 krad	0 > 0 > 0/3	0 > 0 > 0/3	1 > 1 > 2/3
100 krad	0 > 0 > 0/3	0 > 0 > 0/3	2 > 2 > 3/3

Table 3 summarizes the results of gamma and proton radiation endurance tests, respectively. Initial failure assessment measurements were performed right after the irradiation. Additional failure evaluations were performed after a storage at room temperature for 168 h, and after a subsequent storage for additional 168 h at the maximum specified device operation temperature: 85 °C for the suppliers A and C, and 125 °C for the supplier B.

None of the supplier A and B accelerometers failed at any point of the radiation tests, indicating that gamma and proton radiation doses of up to 100–110 krad do not induce any significant immediate or longer-term destructive effects to these accelerometers. Typical relative variation of the accelerometer parameters does not exceed 2–3 % for the supplier A, and 1% for the supplier B, suggesting a better radiation stability of the design B. However, accelerometers from the supplier C exhibit a considerably weaker radiation endurance. They withstand radiation doses of up to 20 krad. When the doses are increased to 50–55 krad some accelerometers exhibit significant deviation of the parameters beyond the failure threshold. Further dose increase to 100–110 krad results in catastrophic failures in almost all design C accelerometers (complete loss of signal).

Internal visual inspection of the failed supplier C devices by optical microscopy reveals no interconnecting wire bonding failures or any kind of mechanical damage to the MEMS structures for both radiation types (gamma and proton). The ceramic packaging base has seen its color changing from white to yellowish-white, indicating an irreversible change in the material, possibly due to the point defects formation. However, the ceramic remains an insulator, suggesting that this change is not responsible for the device malfunction. The absence of wire bonding failures or any kind of mechanical damage to the MEMS structures allows to conclude that the most probable origin for the failures is the ASIC. It is known that the Si-based CMOS components suffer from ionization and displacement effects caused by gamma and proton irradiation [9].

5. Conclusions

In the present work, the reliability assessment of capacitive MEMS accelerometers of 3 different suppliers (codenamed A, B, and C) for their use in space applications was performed. The applied reliability assessment testing program addressed specific severities typical for space missions. Typical failures of the tested MEMS devices were analyzed and failure root causes were identified taking into account the device design consisting of: MEMS structure, ASIC, interconnecting wires, and package.

General analysis of the test results suggests that the most vulnerable MEMS components are interconnects and ASIC. Interconnecting wires

are the weak point when a MEMS device is exposed to high temperatures and/or mechanical stresses caused by, for instance, rapid temperature changes or excessive mechanical shock levels. In such conditions wire detachment and weakening of wire-to-bonding pads connections occurs at much lower load levels, while the MEMS structures are still not affected. Therefore, in order to improve the overall MEMS device performance it is suggested to improve the design by strengthening the interconnecting wires and realizing a reliable and steadfast internal wire bonding. Special attention shall be paid to the solder composition, which shall sustain temperatures higher than 200 °C. MEMS components for space applications shall have hermetic packaging, which will ensure their reliable operation under a broad range of operation pressure conditions. Both hermetically packaged tested accelerometers from the suppliers A and C show a superior performance under variable pressure conditions when compared to non-hermetically packaged accelerometers of the supplier B. A number of tests, such as accelerated electrical endurance, increased voltage limit, and radiation endurance, show that the MEMS device weak point is related to the ASIC robustness. Therefore, for improvement of the MEMS resistance to the aforementioned stress-factors the same approaches shall be pursued as for the improvement of the integrated circuits reliability for space applications [11,12]. Overall results of the performed reliability assessment tests and failure mode analyses suggest that the most specific MEMS components, namely the MEMS structures, themselves do not constitute the failure causes. Usually, other device components, e.g. interconnects, ASIC or packaging, exhibit lower reliability limits to the specific stresses of the space harsh conditions.

Comparative analysis of the three tested accelerometer designs suggests the design A to exhibit the best overall reliability for space-specific application conditions. Design B also shows good robustness. However, its non-hermetic polymeric packaging makes it potentially unsuitable for the direct use for space applications in the current state. Utilization of a hermetic package and improvement of the wire-bonding temperature resistance would significantly improve this design. Accelerometers of the supplier C have a trend of occasional “infant mortality” failures. It is therefore very important to perform burn-in and initial pre-screening for these devices. Another strong weakness for this design is related to a low radiation endurance, which shall be significantly improved.

Acknowledgments

This research has received funding from the European Space Agency under the contract agreement No. 4000109903/13/Nl/PA (MEMS-REAL).

References

[1] H.R. Shea, Reliability of MEMS for space applications, Reliability, Packaging, Testing, and Characterization of MEMS/MOEMS V, vol. 6111, International Society for Optics and Photonics, 2006, p. 61110A, , https://doi.org/10.1117/12.651008.

[2] A.L. Hartzell, M.G. da Silva, H. Shea, Introduction: reliability of MEMS, MEMS Reliability, Springer, Boston, MA, USA, 2011, pp. 1–7, , https://doi.org/10.1007/978-1-4419-6018-4_1 chapter 1.

[3] H.R. Shea, MEMS for pico-to micro-satellites, MOEMS And Miniaturized Systems VIII, vol. 7208, 2009, p. 72080M, , https://doi.org/10.1117/12.810997 International Society for Optics and Photonics.

[4] B. Stark, Failure modes and mechanisms, MEMS Reliability Assurance Guidelines Space Applications, NASA, Pasadena, CA, USA, 1999, pp. 39–42 https://ntrs.nasa.gov/search.jsp?R=20000047448.

[5] B. Stark, B. Kayali, Qualification testing protocol for MEMS, MEMS Reliability Assurance Guidelines Space Applications, NASA, Pasadena, CA, USA, 1999, p. 222 https://ntrs.nasa.gov/search.jsp?R=20000047448.

[6] I. Marozau, Test Programme for Reliability Assessment of MEMS Products (Non-Published), Technical report, CSEM, Neuchatel, Switzerland, 2016.

[7] E.L. Kaplan, P. Meier, Nonparametric estimation from incomplete observations, J. Am. Stat. Assoc. 53 (282) (1958) 457–481, https://doi.org/10.1080/01621459.1958.10501452.

[8] A.L. Hartzell, M.G. da Silva, H.R. Shea, Lifetime prediction, MEMS Reliability, Springer, Boston, MA, USA, 2011, pp. 9–42, , https://doi.org/10.1007/978-1-4419-6018-4_2 chapter 2.

[9] H.R. Shea, Effects of radiation on MEMS, Reliability, Packaging, Testing, and Characterization of MEMS/MOEMS and Nanodevices X, vol. 7928, 2011, p. 79280E, , https://doi.org/10.1117/12.876968 International Society for Optics and Photonics.

[10] R.O. Carlson, Y.S. Sun, H.B. Assalit, Lifetime control in silicon power devices by electron or gamma irradiation, IEEE Trans. Electron Devices 24 (8) (1977) 1103–1108, https://doi.org/10.1109/T-ED.1977.18884.

[11] A. Belous, V. Saladukha, S. Shvedau, Space Microelectronics Volume 2: Integrated Circuit Design for Space Applications, Artech House, 2017 ISBN 978-1-63081-259-1.

[12] G.C. Messenger, Radiation hardening, AccessScience (2014), https://doi.org/10.1036/1097-8542.566850.